

Flat histogram Monte Carlo sampling for mechanical variables and conjugate thermodynamic fields with example applications to strongly correlated electronic systems

Georg Ganzenmüller*

School of Chemistry, University of Edinburgh, West Mains Road, EH9 3JJ Edinburgh, United Kingdom

Grzegorz Pawłowski†

Institute of Physics, A. Mickiewicz University, ulica Umultowska 85, 61-614 Poznań, Poland

(Received 22 April 2008; revised manuscript received 9 August 2008; published 15 September 2008)

We present a general and unifying framework for deriving Monte Carlo acceptance rules which facilitate flat histogram sampling. The framework yields uniform sampling rules for thermodynamic states given by the mechanically extensive variables appearing in the Hamiltonian. Likewise, Monte Carlo schemes which uniformly sample the thermodynamic fields that are conjugate to the mechanical variables can be derived within this framework. We apply these different, yet equivalent sampling schemes to the extended Hubbard model in the atomic limit with explicit electron spin. Results for the full density-of-states, the charge-order parameter distribution, and phase diagrams for different ratios of the on-site Hubbard repulsion and the intersite interaction are presented. A tricritical point at half-filling of the lattice is located using finite-size scaling techniques.

DOI: 10.1103/PhysRevE.78.036703

PACS number(s): 02.70.Tt, 71.10.Fd, 71.45.Lr, 64.60.-i

I. INTRODUCTION

The aim of this paper is twofold: First, we present a unifying description for the derivation of flat histogram Monte Carlo (MC) sampling rules. We investigate two different methods of flat histogram sampling. One algorithm samples thermodynamic states identified by mechanically extensive variables while the other algorithm samples states given by those thermodynamic fields which are conjugate to the mechanically extensive variables. We then study the feasibility and potential advantages of these different methods by applying them to the two-dimensional extended Hubbard model in the atomic limit (AL-EHM) on a square lattice. The wealth of features present in the phase behavior of this model system—first and second order transition lines as well as tricriticality—render it an ideal test case for investigating the usefulness of flat-histogram methods over traditional Boltzmann MC. The latter method samples a single state point in thermodynamic space in one simulation run. While this method shows good error convergence properties, it can be inconvenient to use if many thermodynamic state points have to be sampled, e.g., when a critical temperature is to be located from a maximum in the heat capacity as a function of temperature. If phase diagrams in multiple dimensions are to be mapped out, a large number of traditional Boltzmann MC simulations is required. A solution to this inconvenience is flat-histogram MC algorithms which enable uniform sampling of macroscopic observables such as potential energy E or number of particles N . These observables are mechanical properties which derive from an ensemble average over particular configurations of the system. Many different algorithms exist which facilitate flat histogram sampling of mechanical observables with entropic sampling [1], multica-

nonical sampling [2], and Wang-Landau (WL) [3] sampling being among the most popular variants. The great advantage of such simulations is that a single simulation provides information about, e.g., all possible number densities or energies that the system under study can possibly attain. The uniform sampling also implies that, in contrast to traditional MC, free energy barriers do not cause any sampling problems. A generic scheme for flat histogram MC sampling of mechanically extensive variables with the aid of the WL algorithm will be given here. Because the results of such simulations are relative probabilities of macroscopic states rather than Boltzmann-weighted averages we will also discuss how to analyze these results and compute averages at the desired thermodynamic state point.

On the other hand, it is also possible to sample the thermodynamic fields which are conjugate to the mechanically extensive variables appearing in the partition function with uniform probability. As a thermodynamic field is coupled to a macroscopic observable (e.g., E is coupled to T by a Boltzmann distribution), a broad range of this observable can be visited by sampling a broad range of values for the field. This approach is somewhat similar to parallel tempering, or replica exchange [4–6], but here we present a simple and systematic derivation for such a MC sampling scheme which does not need multiple copies of the same system to be propagated through phase space. However, the advantage of parallel tempering which allows the system to get around (rather than over) free energy barriers is preserved.

We now describe the physical system under study. The AL-EHM derives from the more general extended Hubbard Hamiltonian,

$$\mathcal{H}_{EHM} = \sum_{ij\sigma} t_{ij} c_{i\sigma}^\dagger c_{j\sigma} + U \sum_i n_{i\uparrow} n_{i\downarrow} + W \sum_{ij} n_i n_j - \mu \sum_i n_i, \quad (1)$$

where t_{ij} is the hopping integral between sites i and j , $c_{i\sigma}^\dagger$ ($c_{i\sigma}$) are the creation (annihilation) operators for an electron

*g.ganzenmueller@ed.ac.uk

†gpawlo@amu.edu.pl

with spin $\sigma = \uparrow, \downarrow$, $n_i = n_{i\uparrow} + n_{i\downarrow}$ is the total number of electrons $\{0, \uparrow, \downarrow, \uparrow\downarrow\}$ on the i th site, U represents the on-site and W the intersite Coulomb interactions (here restricted to nearest-neighbors), and μ is the chemical potential. This Hamiltonian represents an effective model for the description of phenomena such as superconductivity, magnetism, or charge density waves [7,8].

The atomic limit is obtained by setting all $t_{ij}=0$, which is a good approximation if the kinetic energy of the electrons is small compared to the Coulomb interaction parameters U and W . It reads

$$\mathcal{H}_{AL-EHM} = U \sum_i n_{D_i} + W \sum_{ij} n_i n_j - \mu \sum_i n_i, \quad (2)$$

where we have introduced the symbol $n_{D_i} = n_i(n_i - 1)/2$ to denote whether lattice site i is occupied with two electrons or not. The AL-EHM is an adequate model for describing charge-ordering (CO) effects of electrons in strongly correlated systems [9]. As such, it has received much attention over the years but some aspects of it, e.g., the parameter range for which discontinuous phase transitions between states of different charge order can be observed and the existence of a low-temperature phase-separated state, are still the subject of ongoing research [10–12].

Despite its formal simplicity, the AL-EHM shows a highly nontrivial phase behavior, including a tricritical point. Depending on the electron concentration $n = \sum_i n_i / L^2$, where L is the lateral size of the square lattice, and the Coulomb repulsions U and W , different spatial distributions of electrons on the lattice are obtained. These are described in terms of a charge-order parameter ϕ which is defined by

$$\phi = \frac{1}{2} |n_A - n_B|, \quad (3)$$

where n_A and n_B are the electron concentrations on sublattices A and B , given by a checkerboard decomposition of the entire lattice. ϕ varies between zero and unity, with the latter describing the fully charge-ordered (HCO) state and the former the nonordered (NO) state. Low-charge order (LCO) is given by $\phi=0.5$. The relative stability of different charge-ordered states strongly depends on temperature and the ratio of on-site repulsion U and intersite interaction zW with z being the number of nearest neighbors. Examples of different charge-ordered states are shown in Fig. 1. At low temperatures, quarter-filling ($n=0.5$) realizes LCO and half-filling of the lattice results in HCO, both as infinite, lattice-spanning domains. Filling fractions which are not integer multiples of $1/4$ result in mixed structures of LCO and HCO which can also occur as lattice-spanning domains. Other configurations with domains that only persist over a few lattice sites are interpreted as NO. Detailed analysis of the percolation problem in this model taking into account finite size effects is presented in previous work by GP [10]. It should be noted that the charge-order parameter ϕ roughly coincides with the concentration of doubly occupied lattice sites, i.e., $\phi \approx 2 \sum_i n_{D_i} / L^2$, for n close to unity and $W > 0$. Therefore ϕ is coupled in this regime to the Hamiltonian which implies that

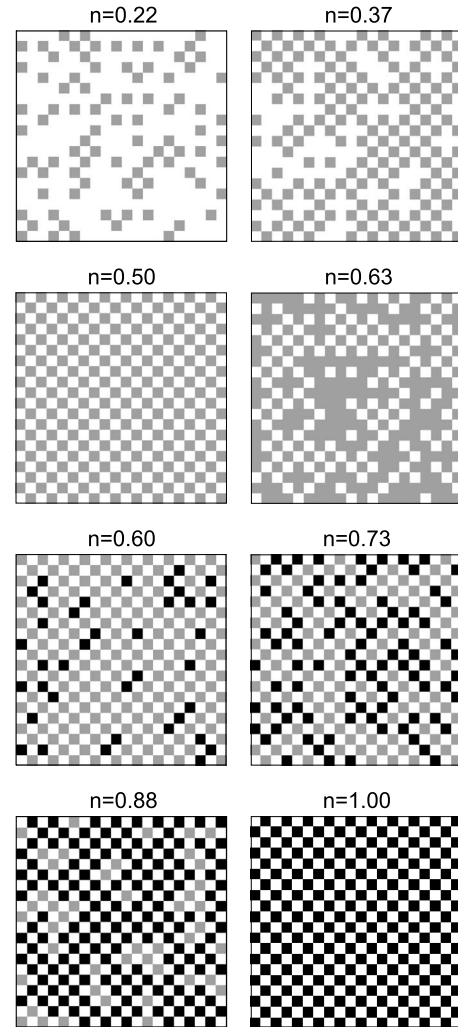


FIG. 1. Exemplary projections of the checkerboard states at finite temperature. Denotations: gray squares—one electron per site, black—two electrons per site, and white—empty site. Note that the projection for $n=0.63$ is exclusively observed for $U/zW > 1.0$ and the lowest four states only for $U/zW < 1.0$.

transitions between states of different charge order will be accompanied by the usual signs indicating a thermodynamic phase transition such as a peak in the heat capacity or the compressibility.

The AL-EHM Hamiltonian and that of the well-known Blume-Capel (BC) model [13] are formally very similar as both describe decorated lattice-gas models. However, we wish to emphasize that mapping of Eq. (2) to a pseudospin model is nontrivial due to the two distinct one-electron states of each lattice site, $\{\uparrow, \downarrow\}$, as has been shown in earlier work of GP [10]. Because we consider the electron spin explicitly, the phase diagram of the model considered here will be qualitatively different from the BC model and the one-component lattice gas model using the simplified lattice states $\{0, 1, 2\}$ [11,12]. Inclusion of the electron spin significantly enlarges the space of lattice states as every state with N_1 single-occupied sites is 2^{N_1} -fold degenerated with respect to spin direction. The case with explicit electron spin has

been analyzed within the mean-field approximation [7,8] and studied recently with MC methods [10,14]. Other studies dealing with the extended Hubbard model for the special case $n=1$ can be found in [15,16] or, for the one-dimensional case, in [12].

The rest of this paper is organized as follows: First, a systematic derivation of flat-histogram sampling techniques for either mechanically extensive or intensive field variables appearing in a Hamiltonian is described. We then present results obtained with different variations of these sampling schemes for the selected cases of the ratio $U/zW=0.5$ and 0.8 . These cases are exemplary for second- or first-order transitions between phases of different charge order. The existence of a tricritical point for $n=1$ is confirmed and we investigate tricriticality for general lattice fillings $n \geq 1$. We conclude with a discussion of the results obtained in this study and the usefulness of different variations of flat-histogram sampling.

II. FLAT HISTOGRAM SAMPLING STRATEGIES

In this section we derive MC transition probabilities which facilitate a random walk either in the space spanned by mechanically extensive variables or in a space given by the thermodynamic fields conjugate to the mechanically extensive variables.

A. Flat histogram sampling of mechanically extensive variables

Consider a general partition function for a lattice system which neglects kinetic energy contributions,

$$\Xi(\beta, \xi) = \sum_{\nu} \exp(-\beta E_{\nu} + \beta \xi X_{\nu}), \quad (4)$$

where the sum runs over all microstates ν in configuration space. $\beta=1/k_B T$ is the inverse temperature, ξ is an external field coupling to a mechanically extensive variable X of the system, and E is the potential energy. In the following we will focus on the case where ξ is the chemical potential μ and X corresponds to the number of particles N , but the same formalism applies to pressure/volume or external magnetic field/magnetization. The microstate probability for any ν is clearly

$$P(\nu, N, E) = \frac{1}{\Xi} \exp(-\beta E_{\nu} + \beta \mu N_{\nu}) \quad (5)$$

and the macrostate probability for observing any particular combination of an energy E' and a number of particles N' is

$$P(N', E') = \frac{1}{\Xi} \sum_{\nu} \delta(N_{\nu} - N') \delta(E_{\nu} - E') \exp(-\beta E_{\nu} + \beta \mu N_{\nu}). \quad (6)$$

Performing the summation in the above equation yields the density of states, or the degeneracy, of the macrostate given by X' and E' :

$$P(N', E') = \frac{1}{\Xi} \Omega(N', E') \exp(-\beta E' + \beta \mu N'). \quad (7)$$

For sampling both extensive properties of the system with uniform probability we need to define a *biased* microstate probability.

$$\tilde{P}(\nu, N, E) = \frac{P(\nu, N, E)}{P(N, E)} = \frac{1}{\Omega(N, E)}. \quad (8)$$

It is easily verified that the above expression samples both E and N with uniform, i.e., constant, probability by looking at the corresponding expression for the biased macrostate probability:

$$\tilde{P}(N, E) = \sum_{\nu} \tilde{P}(\nu, N, E) = \text{const.} \quad (9)$$

MC transition probabilities which realize such a flat histogram sampling are obtained from the detailed balance condition [17] and its Metropolis solution [18]. The MC acceptance probability for moving from old microstate o to a new microstate n reads

$$P_{acc}(o \rightarrow n) = \min \left[1, \frac{\tilde{P}(\nu_n, N_n, E_n)}{\tilde{P}(\nu_o, N_o, E_o)} \right] = \min \left[1, \frac{\Omega(N_o, E_o)}{\Omega(N_n, E_n)} \right]. \quad (10)$$

We can now intuitively understand how flat-histogram sampling schemes work in general: Dividing a Boltzmann weighted microstate probability such as Eq. (5) by its corresponding macrostate probability yields a new probability which is uncoupled from the thermodynamic fields which affect the Boltzmann distribution. Hence a random walk in the space given by E and N is performed.

Unfortunately, we cannot employ a sampling scheme like Eq. (10) directly because the $\Omega(N, E)$ are unknown in general. It is here where the WL algorithm [3] comes in as it provides a convenient route to finding $\Omega(N, E)$ in a self-consistent way. At the beginning of the simulation, an initial guess is made, e.g., $\Omega(N, E) = \text{const} \forall (N, E)$. As the simulation proceeds, the current estimates of $\Omega(N, E)$ are used for determining whether a trial move is accepted or not. Whenever a specific state (N', E') is sampled, $\Omega(N', E')$ is updated through the operation $\Omega(N', E') \rightarrow f \times \Omega(N', E')$, where f is an arbitrary convergence factor greater than unity. Also, a histogram of visited states $H(N, E)$ is kept during the course of the simulation. Due to the dynamic updating of $\Omega(N, E)$, the simulation is always pushed away from the current state in the next move and $H(N, E)$ will eventually become flat. When this is the case f is reduced, e.g., by letting $f = \sqrt{f}$ and $H(N, E)$ is reset to zero. The simulation is run until f reaches a value f_{\min} which is arbitrarily close to unity so that future updates of $\Omega(N, E)$ become negligible. It is important to note that detailed balance is violated at the beginning of the simulation when f is sufficiently large so that updates of $\Omega(N, E)$ are non-negligible. However, once the $\Omega(N, E)$ are reasonably converged we can set $f=1$ and start accumulating averages for any information we wish to extract from the visited microstates $\nu(N, E)$. These averages

can then be reweighted to Boltzmann-weighted ensemble averages at arbitrary values of the conjugate thermodynamic fields β and μ as will be explained further below.

We can extend the sampling method which was described above for all mechanically extensive variables appearing in the partition function to the case where one of these variables is sampled according to a Boltzmann distribution while the other variable is sampled uniformly. The starting point for this is again a microstate probability in the grand-canonical ensemble

$$P(\nu, N, E) = \frac{1}{\Xi} \exp(-\beta E_\nu + \beta \mu N_\nu). \quad (11)$$

Suppose we want to sample all particle numbers with uniform probability but we wish to maintain a Boltzmann distribution of energies for each N . We thus define the macrostate probability for observing N' particles at fixed temperature as

$$\begin{aligned} P(N') &= \frac{1}{\Xi} \sum_\nu \delta(N_\nu - N') \exp(-\beta E_\nu + \beta \mu N_\nu) \\ &= \frac{1}{\Xi} \exp(\beta \mu N') Q(N'), \end{aligned} \quad (12)$$

where $Q(N)$ is the canonical partition function for N particles at inverse temperature β . The biased microstate probability reads

$$\tilde{P}(\nu, N, E) = \frac{P(\nu, N, E)}{P(N)} = \frac{\exp(-\beta E_\nu)}{Q(N)}, \quad (13)$$

which results in the following Metropolis MC acceptance rule for particle insertion or deletion:

$$P_{acc}(N_o \rightarrow N_n) = \min \left\{ 1, \frac{\exp[-\beta E(N_n)] Q(N_o)}{\exp[-\beta E(N_o)] Q(N_n)} \right\}. \quad (14)$$

The $Q(N)$ can be determined again by means of the WL algorithm. This sampling scheme was first mentioned in [19] where it was used to calculate the chemical potential. In [20,21] and very recently in [22] it has been applied to first order phase transitions with great success.

Note that the particular form of the Hamiltonian equation (2) lends itself to yet another sampling strategy: The Hubbard on-site repulsion parameter U is coupled to the number of doubly occupied lattice sites (doublets) just as the chemical potential is coupled to the number of electrons on the lattice. It is therefore straightforward to perform a WL sampling scheme at fixed n and T which samples all possible numbers of doublets N_D uniformly:

$$P_{acc}(N_{D_o} \rightarrow N_{D_n}) = \min \left\{ 1, \frac{\exp[-\beta E(N_{D_n})] Q(N_{D_o})}{\exp[-\beta E(N_{D_o})] Q(N_{D_n})} \right\}. \quad (15)$$

Similar to the uniform sampling of N , the *field* U coupled to the number of doublets N_D does not appear in the MC acceptance rule and the canonical partition functions $Q(N_D)$ have to be determined iteratively.

B. Random walk in thermodynamic field space

As pointed out in the Introduction, it is also possible to define microstate transition probabilities which will effect a random walk in thermodynamic field space. To derive such probabilities, we start from the following *über* partition function:

$$\Psi = \int_{\beta_{min}}^{\beta_{max}} \int_{\mu_{min}}^{\mu_{max}} d\beta d\mu \sum_\nu \exp(-\beta E_\nu + \beta \mu N_\nu), \quad (16)$$

where the ensemble definition incorporates not only the mechanical configurations that the system can attain but also a range of the fields temperature and chemical potential. In exact analogy to the above derivation we define the microstate probability for any element of this ensemble,

$$P(\nu, \mu, \beta) = \frac{1}{\Psi} \exp(-\beta E_\nu + \beta \mu N_\nu), \quad (17)$$

and a corresponding macrostate probability

$$P(\mu, \beta) = \sum_\nu P(\nu, \mu, \beta) = \frac{1}{\Psi} \Xi(\mu, \beta), \quad (18)$$

which is of course proportional to the grand partition function $\Xi(\mu, \beta)$. The *biased* microstate probability is again obtained by dividing the microstate probability through the macrostate probability:

$$\tilde{P}(\nu, \mu, \beta) = \frac{P(\nu, \mu, \beta)}{P(\mu, \beta)} = \frac{\exp(-\beta E_\nu + \beta \mu N_\nu)}{\Xi(\mu, \beta)}. \quad (19)$$

We can show that this biased microstate probability indeed corresponds to an ensemble in which the probability for observing any μ and β is uniform.

$$\tilde{P}(\mu, \beta) = \sum_\nu \tilde{P}(\nu, \mu, \beta) = 1. \quad (20)$$

MC transition probabilities for a move from an old state (μ_o, β_o) to a proposed new state (μ_n, β_n) while maintaining the current configuration ν are obtained by inserting Eq. (19) into the detailed balance condition and using the Metropolis solution:

$$\begin{aligned} P_{acc}(o \rightarrow n) &= \min \left[1, \frac{\tilde{P}(\nu, \mu_n, \beta_n)}{\tilde{P}(\nu, \mu_o, \beta_o)} \right] \\ &= \min \left[1, \frac{\exp(-\beta_n E_\nu + \beta_n \mu_n N_\nu) \Xi(\mu_o, \beta_o)}{\exp(-\beta_o E_\nu + \beta_o \mu_o N_\nu) \Xi(\mu_n, \beta_n)} \right]. \end{aligned} \quad (21)$$

The weights $\Xi(\mu, \beta)$ which appear in this sampling scheme are unknown *a priori* and need to be determined self-consistently during the course of the simulation with the WL algorithm. To do this, we choose discrete values of μ and β which we wish to sample and start out with a uniform guess for all $\Xi(\mu, \beta)$. We let the system evolve in the current state (μ, β) by a normal Boltzmann-weighted MC scheme and attempt changes in μ or β at fixed intervals. After such a change—irrespective of whether it has been accepted or not—the current value of $\Xi(\mu, \beta)$ is modified by letting

$\Xi(\mu, \beta) = f \times \Xi(\mu, \beta)$ where f is greater than unity. Also a histogram $H(\mu, \beta)$ is kept which serves as an indicator for when to reduce the value of f . Once we deem $H(\mu, \beta)$ to be sufficiently flat we reduce f by $f = \sqrt{f}$ and reset the histogram to zero. This process is iterated until f is arbitrarily close to unity. When this is the case, we stop updating $\Xi(\mu, \beta)$ so that detailed balance is recovered. The simulation will now perform a random walk in μ and β and we can accumulate unbiased averages of quantities such as E and N for all states (μ, β) by means of Boltzmann MC sampling. The whole simulation is therefore a combination of a thermodynamic field random walk and standard MC.

Simulation results presented in this paper have made use of the above formalism in order to sample a rectangular grid given by a range of different values for temperature and chemical potential. Extension to sampling only one thermodynamic field is straightforward. We have also employed such a scheme which only varies the temperature at a fixed number of occupied lattice sites, thus corresponding to a set of canonical ensembles simulated within a single simulation. In this case we have the MC transition probabilities from old temperature o to new temperature n ,

$$P_{acc}(o \rightarrow n) = \min \left[1, \frac{\exp(-\beta_n E_n) Q(\beta_o)}{\exp(-\beta_o E_n) Q(\beta_n)} \right]. \quad (22)$$

We note that this specific scheme has been first presented in [23] where it was used to find the critical temperature for a 2D Ising model from the peak in the heat capacity c_V . However, the MC transition probabilities were given in an *ad hoc* fashion without any derivation and it is not entirely clear whether these authors obtained c_V from energy fluctuations or from the numerically computed second derivatives of the $Q(\beta)$ with respect to temperature. In the following we abbreviate the conjugate field random walk sampling method as CFRW and, in order to distinguish it from WL sampling of extensive mechanical quantities, we abbreviate the latter as WLEXT.

C. Analysis of results produced by flat-histogram sampling

We can see that the two different approaches—sampling a mechanical quantity or switching the conjugate thermodynamic field with uniform probability and sampling ensemble averages at these states with a Boltzmann distribution—will yield the same information. However, there is one major difference with regards to how ensemble averages over the simulation run are computed. The conjugate field random walk directly delivers the desired Boltzmann weighted ensemble averages for each discrete point in field space. In contrast, if mechanical probabilities are sampled uniformly, the underlying probability distributions are in general non-Boltzmann and we need to “reweight” the actual simulation data to the desired Boltzmann distribution specified by a set of thermodynamic fields such as β or μ . This will be detailed in the following.

The WL algorithm in conjunction with Eq. (10) yields the density of states for all E and N . Grand-canonical ensemble averages of any observable A that depends on E and N can be computed at any desired temperature or value of the chemical potential according to

$$\langle A \rangle_{\beta, \mu} = \frac{\sum_N \sum_E A(E, N) \Omega(E, N) \exp(-\beta E + \beta \mu N)}{\sum_N \sum_E \Omega(E, N) \exp(-\beta E + \beta \mu N)}. \quad (23)$$

Canonical ensemble averages are computed by summing over the subset of the density of states (DOS) corresponding to the desired number of particles N' :

$$\langle A \rangle_{\beta, N'} = \frac{\sum_N \sum_E A(E, N) \delta(N - N') \Omega(E, N) \exp(-\beta E)}{\sum_N \sum_E \delta(N - N') \Omega(E, N) \exp(-\beta E)}. \quad (24)$$

Sampling scheme Eq. (14) which effects a random walk in particle numbers at fixed temperature provides not the DOS but the canonical partition functions depending on N . From these, grand-canonical ensemble averages are obtained for any value of the chemical potential μ :

$$\langle A \rangle_{\mu} = \frac{\sum_N A(N) Q(N) \exp(\beta \mu N)}{\sum_N Q(N) \exp(\beta \mu N)}. \quad (25)$$

In the case of the sampling scheme Eq. (15), where a random walk in the number of doublets at fixed n and T is performed, we have to reweight the converged canonical partition functions to a chosen value of U :

$$\langle A \rangle_U = \frac{\sum_{N_D} A(N_D) Q(N_D) \exp(-\beta U N_D)}{\sum_{N_D} Q(N_D) \exp(-\beta U N_D)}. \quad (26)$$

In the present study we are especially interested in thermodynamic quantities which signal a phase transition. Specifically, we compute the isothermal compressibility κ_T in the grand canonical and canonical ensembles from the fluctuation formula

$$\kappa_T = \frac{\beta \langle N^2 \rangle - \langle N \rangle^2}{\rho \langle N \rangle}, \quad (27)$$

and the full probability distribution of doubly occupied lattice sites:

$$p(N_D) = \frac{Q(N_D) \exp(-\beta U N_D)}{\sum_{N_D} \exp(-\beta U N_D)}. \quad (28)$$

No such reweighting is required for results produced by the random walk in thermodynamic field space. One only needs to keep histograms of the variables of interest, e.g., a histogram of visited E and ϕ in the case that temperature is varied at constant number density. From this information, we can compute the specific canonical heat capacity from the standard fluctuation formula

$$c_V = \frac{\langle E^2 \rangle - \langle E \rangle^2}{(k_B T)^2 N}, \quad (29)$$

and the canonical charge order susceptibility χ_V ,

$$\chi_V = \frac{\langle \phi^2 \rangle - \langle \phi \rangle^2}{N}. \quad (30)$$

III. SIMULATION RESULTS

For notational convenience, we employ reduced units throughout. The intersite interaction parameter W is set to

unity, the on-site Hubbard repulsion is expressed as $U^* = U/4W$, temperature is defined as $T^* = k_B T/W$ with $k_B = 1$, and all energies are given in units of W . Unless otherwise stated, we studied square lattices of lateral length $L=40$. One Monte Carlo cycle (MCC) consists of L^2 MC moves and simulation run time is measured in m MCC. For a description of the MC moves employed see [10]. The results reported in this section have been obtained with a variety of different flat-histogram sampling variations which will be described individually in the context of the respective application.

A. Tricritical behavior at half-filling

It has been observed before [10] that the high-temperature charge-disordered state turns into a charge-ordered state as temperature is lowered. Depending on the value of U this transition is either discontinuous (first-order) or continuous (second-order). In general, the crossover between a first- and second-order phase transition regime implies the existence of a multicritical point [24] which, in this case, is a tricritical point (TCP). At temperatures below the TCP, the system shows phase coexistence between a disordered state and an ordered state which itself is split up into two symmetric phases. The disordered state is characterized by low concentration of doubly occupied sites $m = n_D/L^2$ and a low value of the charge-order parameter ϕ . The ordered state features high concentration of doublets and a high value of ϕ and its two symmetric phases are given by the two checkerboard sublattices on either of which the doublet density is located. A quantitative order parameter which identifies the sublattice is obtained from Eq. (3) by removing the modulus operator: $M = (n_A - n_B)/2$.

As the TCP marks the crossover from a line of first-order transitions to a line of (critical) second-order transitions it is possible to obtain its precise location in the following way [25]: One starts out at a subcritical temperature and finds phase coexistence between the ordered and disordered state by tuning U such that the probability distribution $p(m)$ is bimodal with equal areas under both peaks. The Binder cumulant ratio [26],

$$U_L = 1 - \frac{\langle (m - \langle m \rangle)^4 \rangle}{3 \langle (m - \langle m \rangle)^2 \rangle^2}, \quad (31)$$

is then calculated and this procedure is repeated for a range of different temperatures and system sizes L . Due to the scale invariance of U_L at criticality, all curves of U_L when plotted against the temperature will intersect at a single temperature which is then taken as the estimate of the tricritical temperature.

In order to begin the above procedure it is first necessary to obtain a rough estimate for the parameter range of U and T in which the probability distribution $p(m)$ starts to appear bimodal. We obtained $p(m)$ through WLEXT simulations which sample all possible numbers of doublets at constant temperature and fixed electron concentration [cf. sampling scheme Eq. (15)]. These simulations were run with convergence parameters $f_{initial} = \exp(1)$, $\ln(f_{final}) = 10^{-8}$ and f was reduced as soon as every possible number of doublets that the system can attain had been visited at least 1000 times.

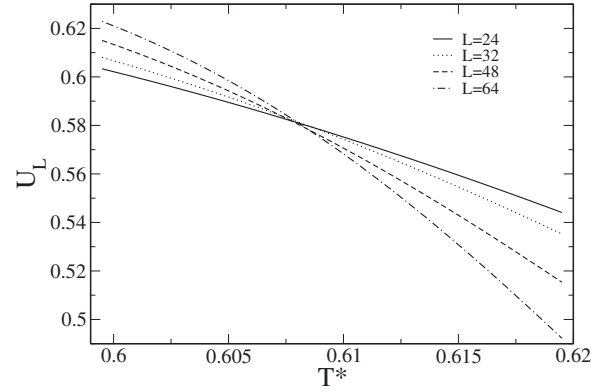


FIG. 2. Binder cumulant ratio U_L in the vicinity of the tricritical point at half-filling for different lattice sizes L .

After the onset of bimodality in $p(m)$ had been conveniently located this way we performed a single long Metropolis MC simulation at this state point for system sizes $L = \{24, 32, 48, 64\}$ and used the histogram reweighting technique [27] to calculate U_L for different temperatures with U chosen subject to the constraint that $p(m)$ satisfied the equal-area rule. The resulting plot of U_L against temperature is shown in Fig. 2: All four curves for different system sizes intersect to within numerical uncertainty at $T_{TCP}^* = 0.6080(4)$ with the uncertainty in the last decimal place given by the standard deviation of the average of the crossing points.

In order to further verify the TCP in this system we invoke the universality of the ordering parameter distribution $p(M)$. Because microscopic details are irrelevant at criticality, the measured form of $p(M)$ will coincide with other model systems featuring a TCP, provided that the distributions are scaled to unit norm and variance. To this end we employ a measured $p(M)$ for the 2D Blume-Capel model as a reference (courtesy of Wilding [25]) and adjust T and U for each system size L such that $p(M)$ collapses on the reference distribution. Results are shown in Fig. 3 where the agreement is clearly excellent. This procedure yields the apparent, i.e., system-size dependent, values of T_{TCP} and U_{TCP} for each value of L , which is to be contrasted with the Binder cumu-

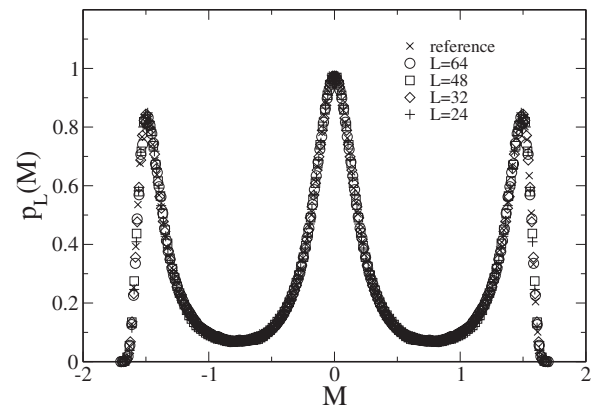


FIG. 3. Ordering parameter distribution $p(M)$ at tricriticality for different lattice sizes and the reference distribution for the 2D Blume-Capel model. All distributions are scaled to unit norm and variance.

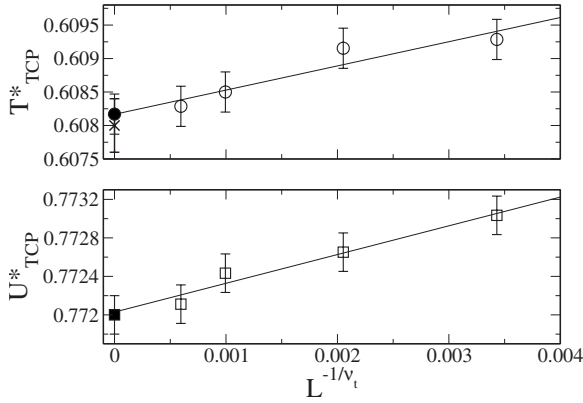


FIG. 4. Upper plot: Finite size scaling plot of the apparent tricritical temperature for different lattice sizes L . Open circles denote simulation results and the straight line represents a least-squares fit to these data points which is used to extrapolate to $L=\infty$ yielding $T_{TCP}^*=0.6082(3)$. The cross marks the estimate for $T_{TCP}^*=0.6080(4)$ obtained from the Binder cumulant intersection method (see text). Lower plot: Open squares denote the apparent value of U_{TCP}^* at tricriticality for different system sizes. Extrapolation to $L=\infty$ using a linear least-squares fit yields $U_{TCP}^*=0.7720(2)$, shown as a closed square. Error bars show the estimated uncertainty in the data points as obtained from the standard deviation of the average from four independent runs.

lant intersection method that yields an estimate for the infinite system tricritical temperature. An estimate for the $L=\infty$ TCP based on the apparent TCP values is obtained from the finite-size scaling relation [27] $T_{TCP}(L)=T_{TCP}(L=\infty)+\lambda L^{-1/\nu_t}$ where λ is a model dependent constant and ν_t is the tricritical scaling exponent which we take to be $\nu_t=0.56$ [28]. Plots of $T_{TCP}(L)$ and $U_{TCP}(L)$ against L^{-1/ν_t} are shown in Fig. 4. Extrapolation of these data points to $L=\infty$ yields $T_{TCP}^*=0.6082(3)$ which agrees with the Binder cumulant estimate to within error and $U_{TCP}^*=0.7720(2)$.

It is interesting to ask what happens to the lines of phase transitions and the TCP at electron concentrations different from half-filling. We found that a perfect match of $p(M)$ onto the tricritical reference distribution is only possible at half-filling and the deviation between the measured distribution and the reference becomes larger the further the density deviates from half-filling. This indicates that a TCP exists only at half-filling but does not rule out the existence of a different type of multicritical point such as a critical end point at other electron concentrations. While it was not possible to identify the exact nature of these multicritical points using our methodological apparatus, we note that the onset of a bimodal distribution in $p(m)$ shifts to lower temperatures as the density is reduced and no bimodal distribution could be observed for $n<0.8$, which can be explained in terms of a vanishing interfacial tension between the two phases of different charge order: A first-order transition can only occur if the coexisting phases are separated by an interface which constitutes a free-energy barrier that stabilizes the phases against mixing with each other. By changing the electron concentration to values beyond $n=1$ one introduces single occupied sites or holes in the lattice which hinder the formation of an interface and thus promote mixing, resulting in a

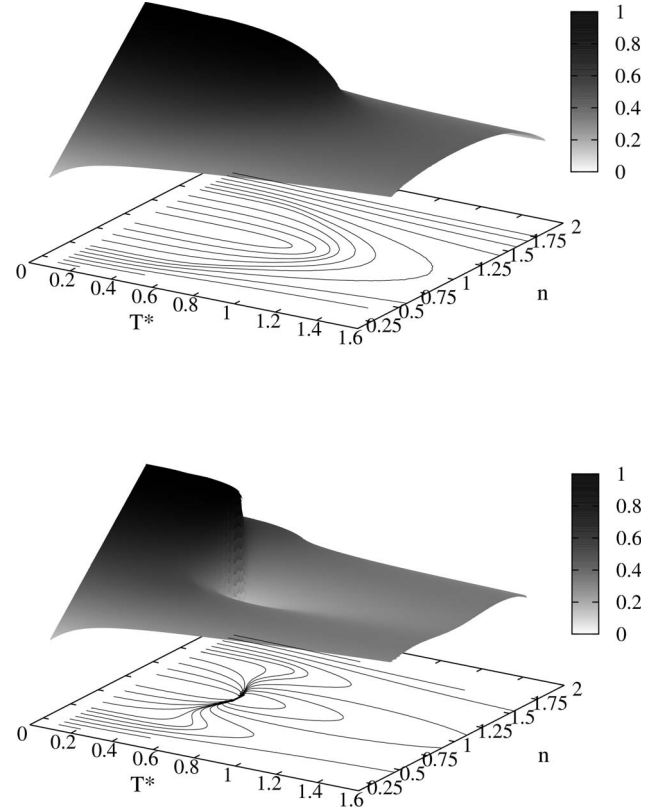


FIG. 5. Charge-order parameter ϕ as a function of density and temperature for $U^*=0.5$ (top) and $U^*=0.8$ (bottom). Projected solid lines indicate lines of constant charge-order parameter.

continuous transition between states of different charge order as U is varied. We conclude this analysis by noting that a line of multicritical points exists in the n - T plane which extends from an upper tricritical temperature at $n=1$ to a vanishing multicritical temperature at $n\approx 0.8$. Therefore first-order phase transitions between states of different charge order can only be observed at temperatures and densities below this line (cf. the global phase diagram Fig. 12).

B. Global order parameter distribution

The charge-order parameter as a function of temperature and density has been obtained using the CFRW sampling scheme Eq. (21) for the range $\mu=[-1.0\dots 12.0]$, $T^*=[0.1\dots 1.6]$ with discretization $\Delta\mu=0.1$ and $\Delta T^*=0.01$. Attempts to change either μ or T were performed once every 2 MCC. The WL convergence procedure of the weights $\Xi(\mu, \beta)$ was initiated with $f_{initial}=\exp(10)$ and f was reduced according to $f=\sqrt{f}$ once every state (μ, β) had been visited a minimum of 100 times. The weights were converged down to $\ln(f_{final})=10^{-6}$ before a histogram of ϕ was accumulated for each thermodynamic state point (μ, β) during a production run of length 1000 mMCC. Results for the charge-order parameter in the T - n plane are shown in Fig. 5 for $U^*=0.5$ and 0.8. These selected cases of the on-site Hubbard repulsion behave quite differently: For $U^*=0.5$ no abrupt transitions between different charge orders can be seen, while for $U^*=0.8$ a steplike change of ϕ along the half-filling line can

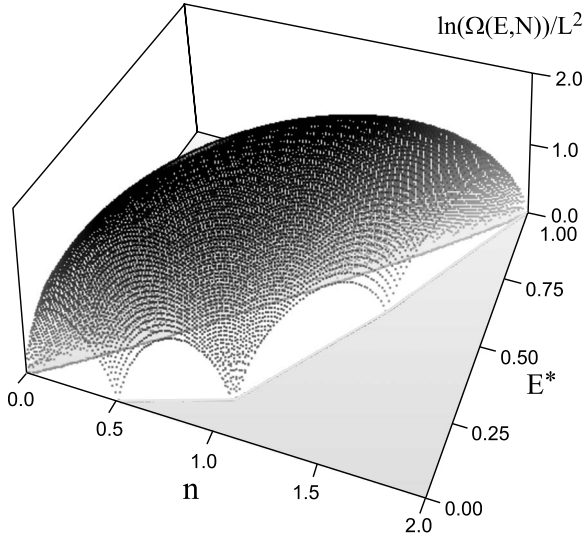


FIG. 6. Density of states for $U^*=0.8$ on a logarithmic scale. $E^*=E/E_{max}$ denotes the fractional energy with respect to the maximum energy possible for this lattice size.

be observed. As discussed above, this agrees with the value of the critical on-site repulsion $U_{TCP}^*=0.7720(2)$ below which the transition occurs continuously for all densities.

C. Density of states and thermodynamic quantities

The full density of states for $U^*=0.8$ and 0.5 has been obtained for a lattice size $L=20$. While this approach allows the calculation of thermodynamic quantities at arbitrary state points, it was only possible to converge the WLEXT algorithm for this two-dimensional sampling problem [cf. Eq. (10)] for small systems. We note that, compared to existing WLEXT simulations of both E and the magnetization M for the Ising model [29] on square lattices, the accessible configuration space of our Hamiltonian is much larger. For a given lattice size L , one has $2^{(L^2)}$ more states in the present model with four lattice site states than for the Ising model. In order to obtain the DOS with high accuracy we resorted to a tighter converge criterion compared to above: The ratio of any entry in the histogram of visited states was required to be within a 15% interval of the mean value of the histogram. $f_{initial}$ was set to $\exp(1)$ and the simulation was stopped at $\ln(f_{final})=10^{-8}$. The total run time required was on the order of 10 000 mMCC which translates into 10 CPU days on a single 2.0 GHz processor.

Figure 6 shows the DOS surface which is spanned over the trivial points 0, 1/4, 1/2, 3/4, and full filling of the lattice. The corresponding entropy $s=S/L^2$ in the canonical ensemble is shown in Fig. 7. Again, the trivial commensurate lattice fillings can be seen but also a region with a steplike drop at the half-filling line is identified. Because $(\frac{\partial s}{\partial T})_V = c_V/T$ this is indicative of a discontinuous transition involving latent heat. As discussed above, the DOS contains all information necessary to calculate all thermodynamic potentials. For a fixed number of electrons, we have the internal energy

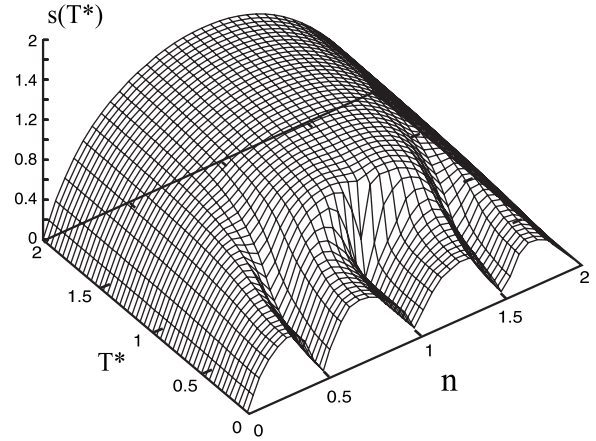


FIG. 7. Entropy per lattice site for $U^*=0.8$ in the n - T^* plane. The gray area on the half-filling line describes the region of discontinuous phase transition.

$$\langle E_{N'}(T) \rangle = \frac{\sum_E \sum_N \delta(N - N') E \Omega(E, N) \exp(-\beta E)}{\sum_E \sum_N \delta(N - N') \Omega(E, N) \exp(-\beta E)}, \quad (32)$$

the free energy

$$F_{N'}(T) = \frac{\ln[\sum_E \sum_N \delta(N - N') \Omega(E, N) \exp(-\beta E)]}{\beta}, \quad (33)$$

and the entropy

$$S_{N'}(T) = \frac{E_{N'}(T) - F_{N'}(T)}{T}. \quad (34)$$

Figures 8 and 9 show these thermodynamic quantities for $U^*=0.5$ and 0.8 at $n=0.45$ and 0.95 . At the lower density considered here, $n=0.45$, both systems do not attain any significant numbers of doubly occupied lattice sites, simply because there is enough room on the lattice to accommodate all electrons without any nearest neighbors. Therefore their thermodynamic behavior must be largely independent of U as the Hubbard on-site repulsion only makes a negligible contribution to the system's energy. The upper parts of Figs. 8 and 9 indeed confirm this reasoning with a small peak in c_V at $T^* \approx 0.6$ for both systems. This peak indicates a temperature-driven phase transition between the LCO at low T and the completely disordered NO state at high T . In contrast to the low-density behavior, the thermodynamic quantities at $n=0.95$ depend strongly on U . Here, we have the situation that nearest-neighbor interaction competes with the Hubbard on-site interaction and, in the case $U^*=0.8$ we find a strong first-order transition between HCO and NO states indicated by a steplike change of the entropy and a well-defined peak in heat capacity at $T^* \approx 0.54$. For $U^*=0.5$ this peak is much broader and, owing to the system's dependence on U , it is also located at a different temperature $T^* \approx 1.00$.

D. Phase diagrams

Traversal of the boundary between two phases is usually accompanied by an abrupt change of a suitably defined order parameter and a peak in the susceptibility of this order pa-

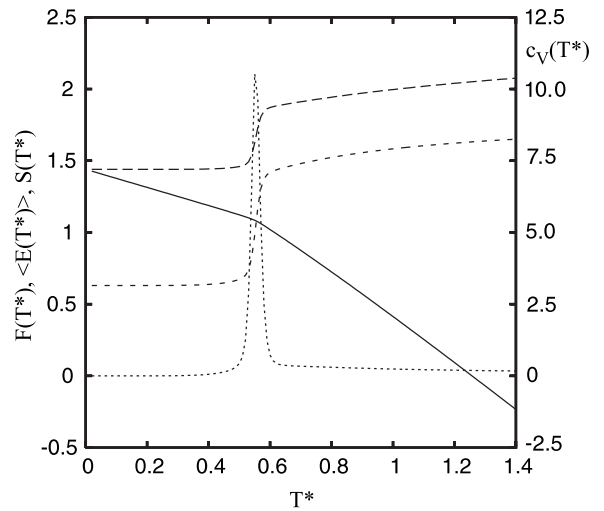
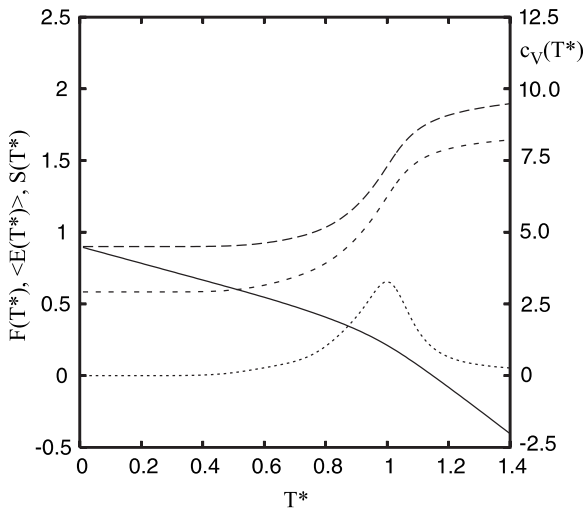
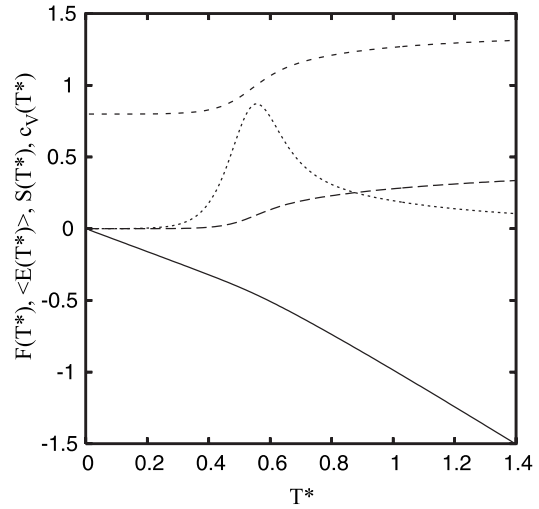
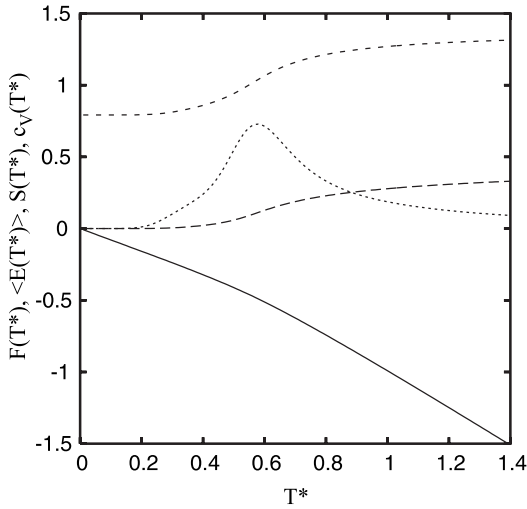


FIG. 8. Thermodynamic quantities per lattice site for $U^*=0.5$. Free energy F —solid line, internal energy E —long dashed line, entropy S —short dashed line, and heat capacity c_V —dotted line. The upper graph is for $n=0.45$ and the lower for $n=0.95$.

FIG. 9. Thermodynamic quantities per lattice site for $U^*=0.8$. Denotations are as for Fig. 8.

parameter. We have used the latter signal to plot the phase diagram in the n - T^* plane for $U^*=0.5$ and 0.8 . Phase boundaries were identified using canonical heat capacities and charge-order parameter susceptibilities from the CFRW sampling scheme at fixed density but varying temperature [cf. sampling scheme Eq. (22)]. Discretization of the temperature range was set to $\Delta T^*=5 \times 10^{-3}$ and the WL convergence parameters used were $f_{initial}=\exp(1)$, and $\ln(f_{final})=10^{-10}$. f was reduced as above once every discrete temperature had been visited 1000 times. A production run of length 10 m MCC was appended after the WL procedure was converged. Histograms of E and ϕ were kept for the subsequent calculation of c_V and χ_V . Complementary to this the isothermal compressibility was computed at fixed temperature from a WLEXT simulation [cf. sampling scheme Eq. (14) which samples all electron concentrations at fixed temperature in a single simulation]. Convergence parameters were as above for the canonical simulations. The converged $Q(N)$ obtained from this simulation enabled us to compute the isothermal compressibility κ_T .

Both phase diagrams are symmetric with respect to mirroring along the half-filling line due to the symmetry of the Hamiltonian equation (2). Figure 10 shows the results for the case $U^*=0.5$. We obtain second-order transitions between

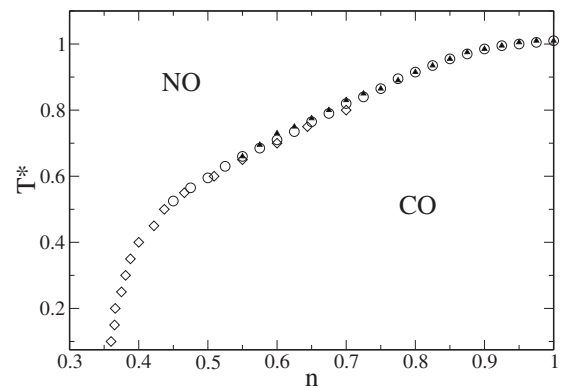


FIG. 10. Phase diagram in the n - T^* plane for $U^*=0.5$. Phase boundaries have been obtained from peaks in c_V (circles), χ_V (triangles), and κ_T (diamonds).

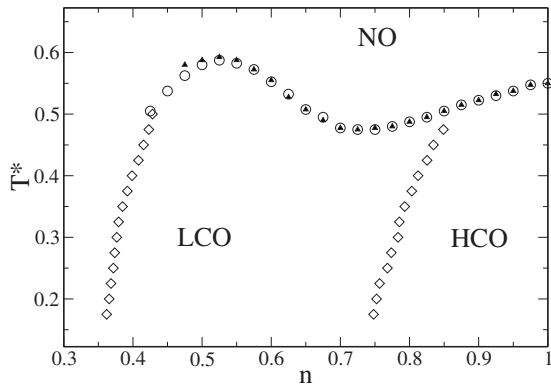


FIG. 11. Phase diagram in the n - T^* plane for $U^*=0.8$. Symbols are as for Fig. 10.

NO and CO. Within the CO phase no indication for an abrupt change of the density or the charge-order parameter was found. The situation for $U^*=0.8$, shown in Fig. 11, is very different: A new line of peaks in κ_T emerges in the CO phase separating it into LCO and HCO regimes. The two sampling schemes used here—CFRW at constant density and WLEXT sampling at a given temperature—constitute already a great improvement over normal Boltzmann MC sampling because they enable us to study an entire temperature or electron concentration range in a single simulation. They are well-suited to determine precisely the location of phase boundaries and require only very modest CPU resources. Nevertheless, we still require several of these simulations to construct an entire phase diagram. This is inconvenient if one wishes to obtain the phase diagram not only as a function of n and T but also depending on U . Ideally, one would perform one large simulation which samples the joint density of states $\Omega(N, E, U)$ which would then allow one to determine the entire phase diagram in the space of density, temperature, and Hubbard interactions. In practice this approach is hardly feasible due to the very long time it would require for the three-dimensional DOS to converge, even for the smallest systems. As noted above, it is already difficult to converge the two-dimensional DOS $\Omega(N, E)$ for medium sized systems. If accuracy and finite-size effects are not of great importance one can resort to the compromise of running multiple very small WL simulations which sample the two-dimensional DOS for specified values of U . This approach is feasible in practice and reduces the number of simulations required to obtain a global phase diagram substantially. Figure 12 shows such a global phase diagram obtained for very small systems and loose WL convergence parameters [$L=8, \ln(f_{final})=10^{-5}$].

IV. DISCUSSION AND CONCLUSION

The development of flat-histogram sampling techniques in general and especially the robust and easy to implement algorithm of Wang and Landau which allows for the iterative determination of the biasing weights needed to accumulate a flat histogram have greatly eased the simulation efforts needed to obtain phase diagrams. In this paper we have em-

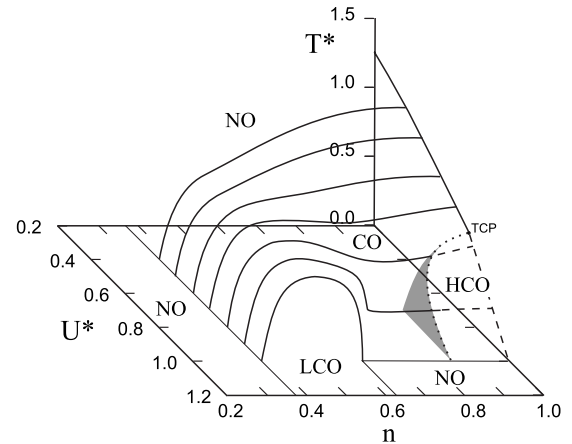


FIG. 12. Global phase diagram. Solid and dashed lines indicate the second- and first-order transitions, respectively, whereas the multicritical points are denoted by a dotted line. The gray area shows the transition LCO-HCO as indicated by peaks in κ_T .

ployed different sampling strategies which either sample mechanically extensive variables such as energy uniformly or perform a random walk in the corresponding conjugate thermodynamic field, e.g., temperature. Depending on the actual system to be studied one might prefer one approach over the other. The advantage of the WLEXT scheme which samples extensive variables is that ensemble averages can be calculated at any thermodynamic state point by simple reweighting. The CFRW scheme on the other hand seems to converge faster but is limited in the chosen discretization width of the thermodynamic fields to be sampled. It has been noted before [30] that the WL algorithm asymptotically reaches a level of uncertainty which does not decrease if the simulation is continued. In comparison, the CFRW scheme employs normal Boltzmann MC sampling for each state point with errors inversely proportional to the square root of the run length. For both algorithms considered, it is possible to sample multiple variables in a single simulation. However, for the WLEXT scheme we and others [21] have found that in practice this is only possible for small systems and it is much more efficient to concentrate the sampling effort on a single variable to be uniformly sampled and run multiple simulations. The CFRW scheme appears to suffer not as much from this drawback but, as noted beforehand, produces less information because it is limited to a certain range and discretization of thermodynamic field variables. On the other hand, there are many cases where only a certain range of, e.g., temperatures is of interest so that CFRW allows one to focus on the relevant range whereas normal WL sampling will need to sample all energies the system can attain because it cannot be determined *a priori* which of these states will have a high Boltzmann weight. This advantage of CFRW is reflected by our simulation timings where it required only a few hours of CPU time to sample a wide range of temperatures and chemical potentials simultaneously whereas it required almost two orders of magnitude longer simulation times for converging the joint DOS using the WLEXT algorithm for a system of only half the size.

Using these flat-histogram schemes we were able to obtain results for the atomic limit of the extended Hubbard

model in a wide range of temperatures and densities and two different values of the Hubbard on-site repulsion. We studied a variant of the Hubbard model with explicit electron spin reflected by the lattice states $\{0, -1, +1, 2\}$ which implies that this model cannot be easily mapped onto simple spin models [10]. In comparison with a study of the classical Hubbard model which considered only the lattice states $\{0, 1, 2\}$ [11], we note that the model studied here differs quantitatively but not qualitatively. The general topology of the phase diagram is not changed with a regime of first-order phase transitions at large values of the Hubbard on-site repulsion U and a regime of continuous transition at low values of U . The effect of the enlarged configurational space due to the inclusion of the electron spin is mainly reflected in a shift of the tricritical point: For half-filling of the lattice we find $T_{TCP}^* = 0.6080(4)$ at $U_{TCP}^* = 0.7720(2)$ while the model with the lattice states $\{0, 1, 2\}$ features a TCP at $T_{TCP}^* = 0.111789(1)$ and $U_{TCP}^* \approx 0.9823$ [11]. Bearing in mind that the regime of discontinuous transition between states of different charge order is bracketed by $T^* = [0, T_{TCP}^*]$ and

$U^* = [U_{TCP}^*, 1]$, we find that this region is much larger for the model studied here than for the simpler model which does not consider the electron spin.

The results agree qualitatively with earlier studies of this model [10, 14], but are much more precise, especially in the region of the discontinuous phase transition. For the first time, we have given a semiquantitative picture of the global phase diagram of this model in a range of physically relevant values of the Hubbard on-site repulsion. Through the use of finite size scaling techniques and mapping to universal ordering parameter distributions we have precisely located a tricritical point at half-filling of the lattice. The question as to what character this multicritical point assumes at different lattice fillings remains open as an interesting topic for future study of this model.

ACKNOWLEDGMENT

G.G. would like to thank P. J. Camp for valuable discussions and critically reading the paper.

-
- [1] J. Lee, Phys. Rev. Lett. **71**, 211 (1993).
 [2] B. A. Berg and T. Neuhaus, Phys. Rev. Lett. **68**, 9 (1992).
 [3] F. Wang and D. P. Landau, Phys. Rev. Lett. **86**, 2050 (2001).
 [4] D. Earl and M. Deem, Phys. Chem. Chem. Phys. **7**, 3910 (2005).
 [5] R. H. Swendsen and J.-S. Wang, Phys. Rev. Lett. **57**, 2607 (1986).
 [6] C. Geyer, in *Computing Science and Statistics: Proceedings of the 23rd Symposium on the Interface* (American Statistical Association, New York, 1991), p. 156.
 [7] R. Micnas, S. Robaszkiewicz, and K. A. Chao, Phys. Rev. B **29**, 2784 (1984).
 [8] R. Micnas, J. Ranninger, and S. Robaszkiewicz, Rev. Mod. Phys. **62**, 113 (1990).
 [9] R. A. Bari, Phys. Rev. B **3**, 2662 (1971).
 [10] G. Pawłowski, Eur. Phys. J. B **53**, 471 (2006).
 [11] T. Misawa, Y. Yamaji, and M. Imada, J. Phys. Soc. Jpn. **75**, 064705 (2006).
 [12] F. Mancini, Eur. Phys. J. B **47**, 527 (2005).
 [13] J. D. Kimel, P. A. Rikvold, and Y.-L. Wang, Phys. Rev. B **45**, 7237 (1992).
 [14] G. Pawłowski and T. Kaźmierczak, Solid State Commun. **145**, 109 (2008).
 [15] M. Bartkowiak, J. A. Henderson, J. Oitmaa, and P. E. de Brito, Phys. Rev. B **51**, 14077 (1995).
 [16] E. Halvorsen and M. Bartkowiak, Phys. Rev. B **63**, 014403 (2000).
 [17] D. Frenkel and B. Smit, *Understanding Molecular Simulation: From Algorithms to Applications*, 2nd ed. (Academic Press, San Diego, 2001).
 [18] N. Metropolis and S. Ulam, J. Am. Stat. Assoc. **44**, 335 (1949).
 [19] Q. Yan, R. Faller, and J. J. de Pablo, J. Chem. Phys. **116**, 8745 (2002).
 [20] J. R. Errington, J. Chem. Phys. **118**, 9915 (2003).
 [21] I. D. Gospodinov and F. A. Escobedo, J. Chem. Phys. **122**, 164103 (2005).
 [22] G. Ganzenmüller and P. J. Camp, J. Chem. Phys. **127**, 154504 (2007).
 [23] C. Zhang and J. Ma, Phys. Rev. E **76**, 036708 (2007).
 [24] I. D. Lawrie and S. Sarbach, in *Phase Transitions and Critical Phenomena*, edited by C. Domb and J. L. Lebowitz (Academic Press, London, 1984), Vol. 9.
 [25] N. B. Wilding and P. Nielaba, Phys. Rev. E **53**, 926 (1996).
 [26] K. Binder, Z. Phys. B: Condens. Matter **43**, 119 (1981).
 [27] D. Landau and K. Binder, *A Guide to Monte Carlo Simulations in Statistical Physics* (Cambridge University Press, Cambridge, England, 2000).
 [28] D. P. Landau and R. H. Swendsen, Phys. Rev. Lett. **46**, 1437 (1981).
 [29] D. P. Landau, S.-H. Tsai, and M. Exler, Am. J. Phys. **72**, 1294 (2004).
 [30] C. Zhou and R. N. Bhatt, Phys. Rev. E **72**, 025701(R) (2005).